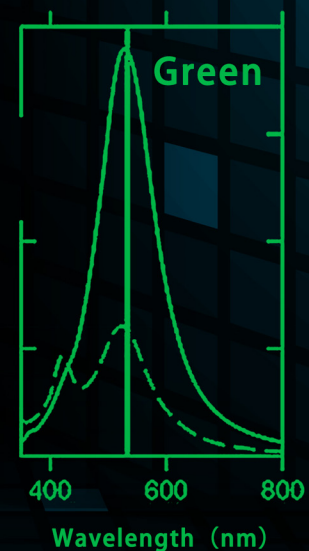
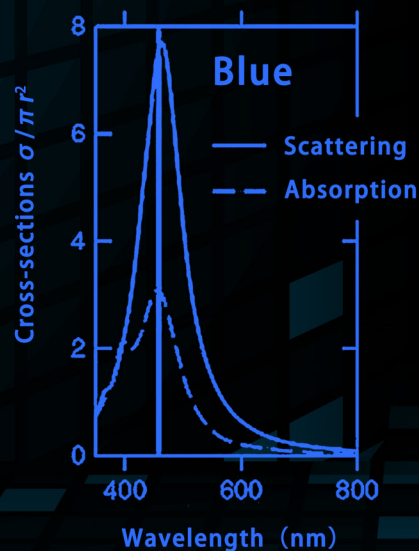
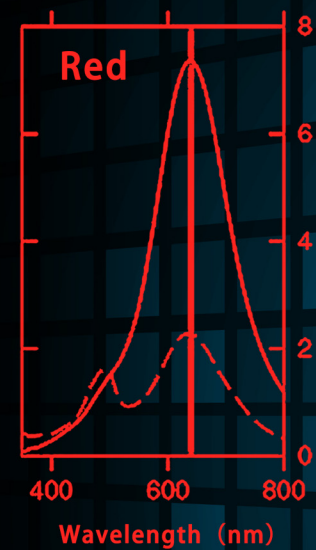
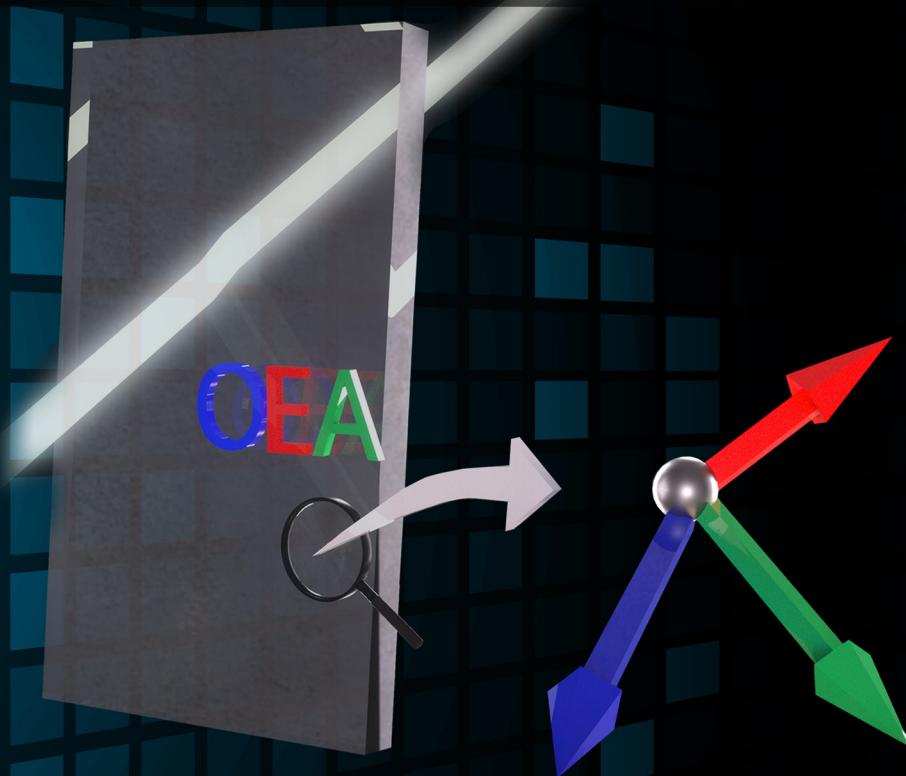


## Toward transparent projection display: recent progress in frequency-selective scattering of RGB light based on metallic nanoparticle's localized surface plasmon resonance

Yiyang Ye, Zhen Liu and Tupei Chen\*

<https://doi.org/10.29026/oea.2019.190020>





DOI: 10.29026/oea.2019.190020

# Toward transparent projection display: recent progress in frequency-selective scattering of RGB light based on metallic nanoparticle's localized surface plasmon resonance

Yiyang Ye<sup>1</sup>, Zhen Liu<sup>2</sup> and Tupei Chen<sup>1\*</sup>

A transparent display simultaneously enables visualization of the images displayed on it as well as the view behind it, and therefore can be applied to, for instance, augmented reality (AR), virtual reality (VR), and head up display (HUD). Many solutions have been proposed for this purpose. Recently, the idea of frequency-selective scattering of red, green and blue light while transmitting visible light of other colours to achieve transparent projection display has been proposed, by taking advantage of metallic nanoparticle's localized surface plasmon resonance (LSPR). In this article, a review of the recent progress of frequency-selective scattering of red, green and blue light that are based on metallic nanoparticle's LSPR is presented. A discussion of method for choosing appropriate metal(s) is first given, followed by the definition of a figure of merit used to quantify the performance of a designed nanoparticle structure. Selective scattering of various nanostructures, including sphere-shaped nanoparticles, ellipsoidal nanoparticles, super-sphere core-shell nanoparticles, metallic nanocubes, and metallic nanoparticles combined with gain materials, are discussed in detail. Each nanostructure has its own advantages and disadvantages, but the combination of the metallic nanoparticle with gain materials is a more promising way since it has the potential to generate ultra-sharp scattering peaks (i.e., high frequency-selectivity).

**Keywords:** light scattering; localized surface plasmon resonance; transparent display

Ye Y Y, Liu Z, Chen T P. Toward transparent projection display: recent progress in frequency-selective scattering of RGB light based on metallic nanoparticle's localized surface plasmon resonance. *Opto-Electron Adv* 2, 190020 (2019).

## Introduction

A transparent display simultaneously enables visualization of the images displayed on it as well as the view behind it. For this reason, transparent display can be applied in augmented reality in which an object appears to be floating in air, shop windows that show vivid images or video for advertisement purpose, and car head-up display where navigation or other information are displayed on a car's windshield. Existing solutions for transparent display include those based on micro-lens array (MLA) systems<sup>1</sup>, projection-based fluorescent display<sup>2</sup>, and organic light emitting diode (OLED) based display<sup>3</sup>, each has its own advantages and subset of applications. Recently, the idea

of frequency-selective scattering of red, green and blue light and transmission of visible light of other colours to achieve transparent projection display has been proposed<sup>4-7</sup>, which takes advantage of metallic nanoparticle's localized surface plasmon resonance (LSPR)<sup>8,9</sup>, and is schematically shown in Fig. 1<sup>10</sup>. This article reviews recent progress of frequency-selective scattering of red, green and blue light that are based on metallic nanoparticle's LSPR<sup>4-7</sup>.

A discussion of method for choosing appropriate metal(s) is first given, followed by the definition of a figure of merit used to quantify the performance of a designed nanoparticle structure. We then review frequency-selective scattering of sphere-shaped nanoparticles,

<sup>1</sup>School of Electrical and Electronic Engineering, Nanyang Technological University, Singapore 639798, Singapore. <sup>2</sup>School of Materials and Energy, Guangdong University of Technology, Guangzhou 510006, China.

\*Correspondence: T P Chen, E-mail: echentp@ntu.edu.sg

Received: 11 June 2019; Accepted: 26 August 2019; Published: 20 December 2019

ellipsoidal nanoparticles, super-sphere core-shell nanoparticles, metallic nanocubes, and finally metallic nanoparticles combined with gain materials.

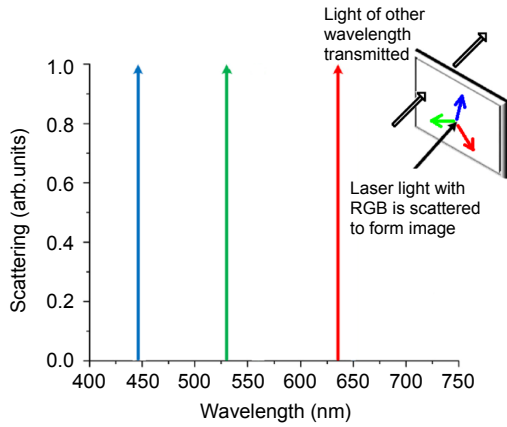


**Fig. 1 | Schematic illustration of the concept of transparent projection display achieved by frequency-selective scattering of red, green and blue light.** This demonstrates the ideal case: light scattering spectrums have ultra-sharp peaks around the central wavelengths of the three additive colours (red, green and blue), while light absorption remains 0 all through the visible light wavelength range. Figure reproduced with permission from Ref.<sup>10</sup>, Optical Society of America.

## Method for choosing metal

Figure 1 shows the ideal case for the transparent projection display based on metallic nanoparticle's LSPR<sup>10</sup>. This method relies on the design of optical resonant scatterers that are strongly frequency-selective in light scattering and have low absorption in the wavelength range of visible light. Metals are chosen by first checking whether they have the potential to generate sharp resonant peak(s) (i.e., strong frequency-selectivity). Two approaches have been proposed for this purpose<sup>4,7</sup>, and they lead to the same conclusion: around interested wavelengths (i.e., wavelengths for red, green and blue light in this case), the dielectric function of a qualified metal should have a small imaginary part or a real part with fast changing rate with respect to wavelength (or frequency).

Both approaches assume quasi-static approximation (i.e., particle size  $\ll$  wavelength) to give a rough estimation. For a metallic nanoparticle of arbitrary shapes, the first approach calculates the ratio of scattering cross section between the on-resonance (at resonant wavelength  $\lambda_0$ ) and off-resonance (at  $\lambda_0 + \Delta\lambda$ , with a small wavelength step  $\Delta\lambda$ ), which is given below<sup>4</sup>:

$$\frac{\sigma_{\text{sca}}(\lambda_0)}{\sigma_{\text{sca}}(\lambda_0 + \Delta\lambda)} \approx 1 + \frac{\left| \text{Re}[\epsilon(\lambda_0 + \Delta\lambda) - \epsilon(\lambda_0)] \right|^2}{\left| \text{Im}[\epsilon(\lambda_0)] \right|^2}, \quad (1)$$

where  $\text{Re}[\cdot]$  and  $\text{Im}[\cdot]$  denote real part and imaginary part of a complex number, respectively, and  $\epsilon(\lambda)$  denotes the metal's dielectric function at a wavelength  $\lambda$ . A sharp scattering peak is equivalent to a large value of the ratio shown in the left-hand-side of equation (1). There-

fore, by observing the right-hand-side of equation (1), it is obvious that a small imaginary part of the metal's dielectric function or a fast-changing real part of the metal's dielectric function generates a sharp scattering peak, and hence a strong frequency selectivity. Derivation of equation (1) is given in Ref.<sup>4</sup>.

The second approach looks at the resonance peak's halfwidth  $\Gamma^*$  (in eV)<sup>7</sup>:

$$\Gamma^* = \frac{2\text{Im}[\epsilon(\omega_0)]}{\sqrt{\left(\frac{d\text{Re}[\epsilon(\omega)]}{d\omega}\right)^2 + \left(\frac{d\text{Im}[\epsilon(\omega)]}{d\omega}\right)^2}}(1 + \beta), \quad (2)$$

where  $\omega$  is incident light's angular frequency ( $\omega = 2\pi c/\lambda$ ,  $c$  is speed of light in vacuum),  $\omega_0$  is the resonant frequency (i.e.,  $\omega_0 = 2\pi c/\lambda_0$ ), and  $\beta$  is usually very small compared to 1 and can be neglected. The two derivatives in the denominator of equation (2) are taken at the resonant frequency  $\omega_0$ . Derivation of equation (2) is given in Ref.<sup>11</sup>. A strong frequency selectivity is equivalent to a narrow width of resonance peak. Thus, by observing equation (2), the second approach reaches the same conclusion as that from the first approach.

So, it is useful to plot  $\eta = \left| \text{Re}\left[\frac{d\epsilon}{d\lambda}\right] / \text{Im}[\epsilon] \right|^2$  in visible

spectrum range (400–800 nm), and choose a metal with a high  $\eta$  value. The  $\eta$  curves of different metals are shown in Fig. 2<sup>4</sup>. It is obvious that silver (Ag) has the largest value for most part of the visible spectrum, while gold (Au) has the largest value around the wavelength of 700 nm. Therefore, Ag is the most suitable candidate for the whole visible spectrum, while Au may be suitable around red light.

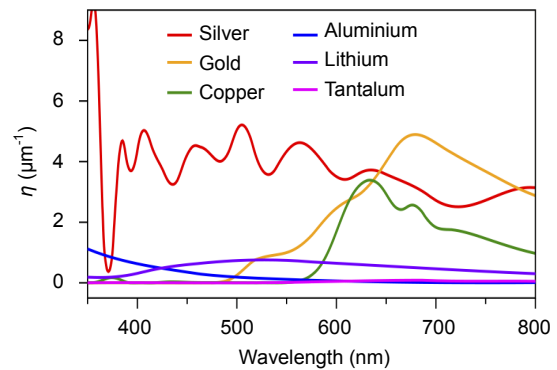


**Fig. 2 |  $\eta$  as a function of wavelength in the visible light range for various metals.** Figure adapted by permission from Ref.<sup>4</sup>, Springer Nature.

## Definition of figure of merit (FOM)

For candidate metals, the next step is to check whether an optimal trade-off between light scattering frequency-selectivity and light absorption can be achieved by tuning its structural parameters (for instance, core diameter, shell thickness for core-shell structure). For the

purpose of tuning structural parameters, it is necessary to quantize the desired performance by a mathematical expression. To achieve this, the following figure of merit (*FOM*) is defined:

$$FOM = \frac{\sigma_{sca}(\lambda_0)}{2\sigma_{sca} + \max\{\sigma_{abs}\}}, \quad (3)$$

where  $\sigma_{sca}$  and  $\sigma_{abs}$  are the scattering and absorption cross sections of a nanoparticle respectively which are affected by the nanoparticle's shape, size, constituent material as well as surrounding medium<sup>8,9</sup>. They can be calculated by the Mie theory for spherical, ellipsoidal and cylindrical shapes<sup>12,13</sup>, or by numerical methods such as FDTD (finite-difference time domain) and DDA (discrete dipole approximation) for arbitrary shapes<sup>14,15</sup>. The overbar and the symbol  $\max\{\sigma_{abs}\}$  respectively denote the mean and the maximum values in the visible spectrum (from 400 nm to 800 nm). This *FOM* is first defined by Soljačić's group<sup>4</sup>, and another two works followed this definition<sup>6,7</sup>. It is obvious from equation (3) that a high value of *FOM* favours the following properties: low absorption cross-section over the whole visible spectrum, a high scattering cross-section at the resonance wavelength, and low scattering cross-section elsewhere, i.e. a narrow or sharp resonance peak. Therefore, the *FOM* suggests that to achieve a high performance, the scatterers should be strongly frequency-selective and have low absorption.

## Nanoparticle structures for frequency-selective scattering

### Sphere-shaped nanoparticles

Sphere-shaped nanoparticle is highly symmetric, and therefore does not need alignment when dispersed in a transparent matrix. Ag nanoparticle's resonance peak wavelength under quasi-static approximation (i.e., particle size  $\ll$  wavelength) is about 416 nm when its sur-

rounding environment has a refractive index of 1.5, according to the resonance condition:  $\text{Re}[\epsilon_m(\lambda_0)] = -2 \cdot \epsilon_s$ <sup>8</sup>, where  $\lambda_0$  is the resonance peak wavelength and  $\epsilon_m(\lambda_0)$  is the metal's dielectric function at this wavelength, and  $\epsilon_s (= n_s^2)$  is the surrounding medium's dielectric function. However, the wavelength ranges for blue, green and red light are 450–490 nm, 520–560 nm and 635–700 nm, respectively<sup>16</sup>. Thus, it is necessary to red-shift Ag nanoparticle's resonance peak wavelength under quasi-static limit into the three wavelength regions of red, green and blue light. For this purpose, two approaches have been proposed: the first one is the core-shell structure with silica as core and silver as shell (Silica/Ag)<sup>4</sup>, and the second one is the core-shell structure with silver as core and TiO<sub>2</sub> as shell (Ag/TiO<sub>2</sub>)<sup>7</sup>. In this section, selective scattering of red, green and blue light based on Silica/Ag is first reviewed, followed by that based on Ag/TiO<sub>2</sub>. The works reported in Refs.<sup>4,7</sup> are summarized below.

### Silica/Ag

For the structure of Silica/Ag, optimization of *FOM* (as defined by equation (3)) is carried out using the multi-level single-linkage algorithm<sup>17</sup>, which can be implemented within the free nonlinear optimization package NLOpt<sup>18</sup>. It was assumed that the transparent matrix (Polyvinyl Alcohol, or PVA in short) in which nanoparticles of Silica/Ag are embedded has a refractive index of 1.44<sup>4</sup>. Refractive index for silica is assumed to be 1.45 and dielectric constants for Ag is from Ref.<sup>19</sup>. However, it should be pointed out that direct usage of Ag's dielectric constants from reference is not appropriate, as this omits effect of surface dispersion of conduction electrons which increases light absorption and decreases light scattering<sup>20,21</sup>, and this effect is numerically demonstrated later in the section: "Spheroidal nanoparticles".

Optimized results from Silica/Ag are shown in Fig. 3 as well as Table 1<sup>4</sup>.

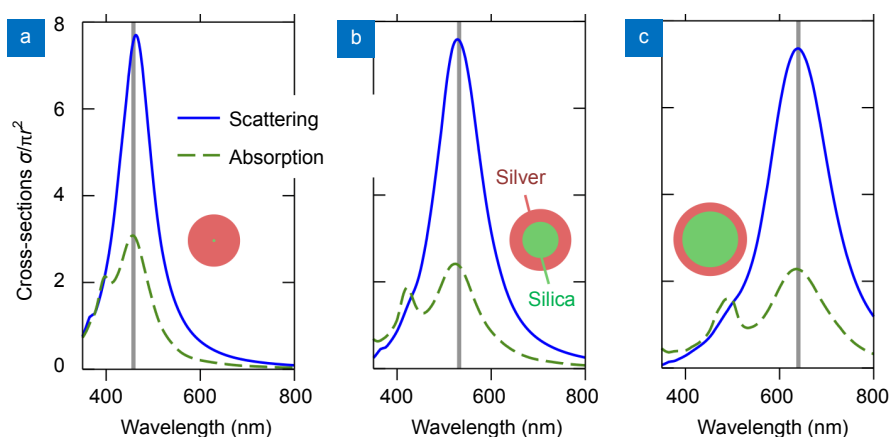


**Fig. 3 | Calculated scattering and absorption cross-sections for Silica/Ag nanoparticles (embedding medium has a refractive index of 1.44).** And optimizations are performed for them to scatter monochromatic light at (a)  $\lambda_0=458$  nm (blue), (b) 532 nm (green), and (c) 640 nm (red). Relative sizes of the structures are shown by the insets; and  $r$  denotes the outer radius of the particle. Figure adapted by permission from Ref.<sup>4</sup>, Springer Nature.

**Table 1 | Optimal particle sizes and FOM for silica-core silver-shell nanoparticles.**

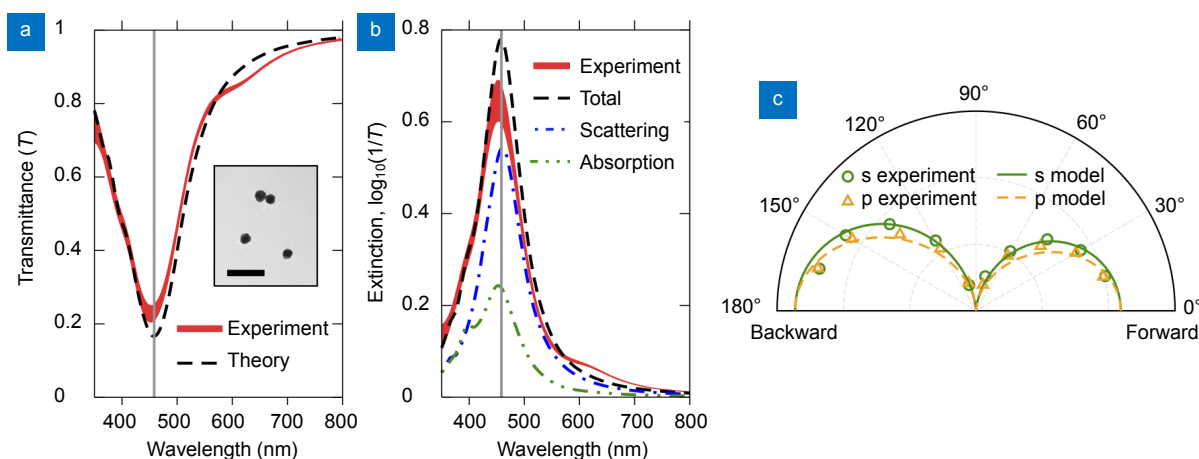
Wavelength $\lambda_0$	Core radius	Shell thickness	FOM
458 nm	1.3 nm	30.8 nm	1.01
532 nm	22.2 nm	15.8 nm	0.91
640 nm	34.3 nm	11.0 nm	0.81

Table adapted by permission from Ref.<sup>4</sup>, Springer Nature.

Due to difficulty in precise synthesis of Silica/Ag structure<sup>22</sup>, experimental verification was conducted only for blue-color-only transparent projection display with spherical Ag nanoparticles with average diameter of ~62 nm (silica core with radius of 1.3 nm is omitted)<sup>4</sup>. A blue-color-only transparent projection display was made by embedding spherical Ag nanoparticles with average diameter of 62 nm into PVA polymer-matrix<sup>4</sup>. This film has a thickness of 0.46 mm, and the areal concentration of Ag nanoparticles is about  $6 \times 10^9/\text{cm}^2$ , or an equivalent

mass concentration of  $7 \mu\text{g}/\text{cm}^2$ . As shown in Figs. 4(a) and 4(b)<sup>4</sup>, the measured transmittance and extinction spectrum agrees well with the results from simulations. The simulated results of light scattering and absorption in Fig. 4(b) indicates that on-resonance scattering is significantly stronger than the on-resonance absorption<sup>4</sup>, which may not remain true if effect of surface dispersion of conduction electrons is included. Angular distribution of scattered light shown in Fig. 4(c) indicates that the scattering is very isotropic and polarization-independent<sup>4</sup>. And these suggest the scattered light from the display can be viewed from a wide angle and the display can be operated with incident light with arbitrary polarization.

In Fig. 5<sup>4</sup>, the transparent projection display at work is shown. The projected image shows up clearly on the display embedded with Ag nanoparticles. In comparison, the same image projected onto regular glass (photo on the right) can barely be seen due to the lack of scattering.



**Fig. 4 | Characterization of the transparent projection film made by dispersing Ag nanospheres with average diameter of 62 nm in PVA.** (a) Comparison of the measured and theoretically calculated transmittance spectrums. The width of the experimentally measured curve stands for one standard deviation over different wavelength of incident light. Inset is a TEM image of the Ag nanospheres with average diameter of  $62 \pm 4$  nm. Scale bar of the TEM image is 200 nm. (b) Comparison of extinction spectrums from experimental measurement and theoretical calculation, and the theoretically calculated scattering and absorption are also shown. (c) Angular distribution of light scattering at the wavelength of 458 nm, with electric field of the normally incident light polarized parallel (p) and perpendicular (s) to the scattering plane. Figure adapted by permission from Ref.<sup>4</sup>, Springer Nature.

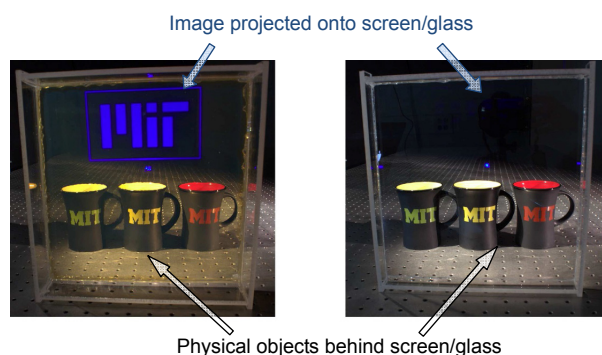


**Fig. 5 | Comparison of the transparent projection display in work (left) with a normal piece of glass (right).** A blue MIT icon is projected onto both the transparent projection display and the normal glass by a laser projector (MicroVision SHOWWX+, wavelength of blue light is  $458 \pm 2$  nm). The image can be viewed clearly on the transparent projection display, but not on the normal glass. Three cups with letters of red, green and yellow colors are placed behind the screen to intuitively demonstrate the transparency. Figure adapted by permission from Ref.<sup>4</sup>, Springer Nature.

**Ag/TiO<sub>2</sub>**

Another way of red-shifting Ag's resonance peak wavelength is by coating Ag nanosphere with a high-index dielectric shell<sup>8</sup>, such as TiO<sub>2</sub>, as reported in another work<sup>7</sup>.

For the structure of Ag/TiO<sub>2</sub>, optimization of its *FOM* is similar to that of Silica/Ag. It was assumed that the transparent matrix (PVA) in which nanoparticles of Ag/TiO<sub>2</sub> are embedded has a refractive index of 1.5<sup>7</sup>. Refractive index for TiO<sub>2</sub> is assumed to be 1.8. The reason why a low refractive index for TiO<sub>2</sub> is chosen rather than a value of 2.7<sup>23</sup> is that the chemical method employed produces amorphous TiO<sub>2</sub> shell<sup>24</sup>, which usually has a much lower refractive index than that of rutile phase due to lower density<sup>25</sup>. The dielectric function of Ag has included the effect of surface scattering of conduction electrons since the silver core's size is comparable to electron's mean free path in bulk silver, which is about 52 nm<sup>21</sup>. The extra damping  $\gamma_s$  caused by surface scattering of electrons is added to the bulk damping  $\gamma_b$  to give the corrected dielectric function  $\epsilon_C$  for silver nanoparticles:

$$\epsilon_C = \epsilon_{exp} + \frac{\omega_p^2}{\omega(\omega + i\gamma_b)} - \frac{\omega_p^2}{\omega[\omega + i(\gamma_b + \gamma_s)]} \quad (4)$$

where  $\epsilon_{exp}$  is silver's dielectric function from Ref.<sup>19</sup> (experimentally determined),  $\omega_p$  is the plasma frequency of silver,  $\omega$  is the frequency of the incident light, and  $i$  is the imaginary number. In the optimization,  $\omega_p$  and  $\gamma_b$  are assumed to be 9.6 eV and 22.8 meV, respectively<sup>26</sup>. And  $\gamma_s$  is given by<sup>27</sup>:

$$\gamma_s = \frac{Av_F}{r} \quad (5)$$

where  $v_F=1.39 \times 10^6$  m/s is the electron velocity at the Fermi surface for silver<sup>26</sup>, and  $r$  is the radius of the silver core,  $A$  is a dimensionless fitting number, whose value is not free from controversy: values from 0.1 to 2 have been theoretically justified<sup>28</sup>. Since  $A$  values of 0.25 and 0.8 have been experimentally reported<sup>27,28</sup>, an  $A$  value of 0.5 is chosen in the optimization.

As the blue-color-only transparent projection display has been demonstrated in Ref.<sup>4</sup> and discussed above, the following discussion will only focus on selective scattering of green light and red light based on Ag/TiO<sub>2</sub>. Optimized results of Ag/TiO<sub>2</sub> are shown in Fig. 6 and Table 2<sup>7</sup>.

**Table 2 | Optimal particle sizes and *FOM* for silver-core TiO<sub>2</sub>-shell nanoparticles.**

Wavelength $\lambda_0$	Core radius	Shell thickness	<i>FOM</i>
525 nm	35 nm	14 nm	0.8941
620 nm	37.5 nm	39 nm	0.8921

Table reproduced by permission from Ref.<sup>7</sup>, The Royal Society of Chemistry.

Due to the difficulty in coating thick TiO<sub>2</sub> shell (i.e., it is difficult to control uniformity of the shell thickness), only the structure for selective scattering of green light was synthesized for experimental verification in the work reported in Ref.<sup>7</sup>. The nanoparticles used for experimental verification have average diameter of 67 nm and average shell thickness of 18 nm (Fig. 7)<sup>7</sup>, which are different from the optimized values. This is due to the difficulty in precisely controlling the sizes of both the core (the core diameter shrinks during the synthesis process) and shell. Nevertheless, the nanoparticles with average

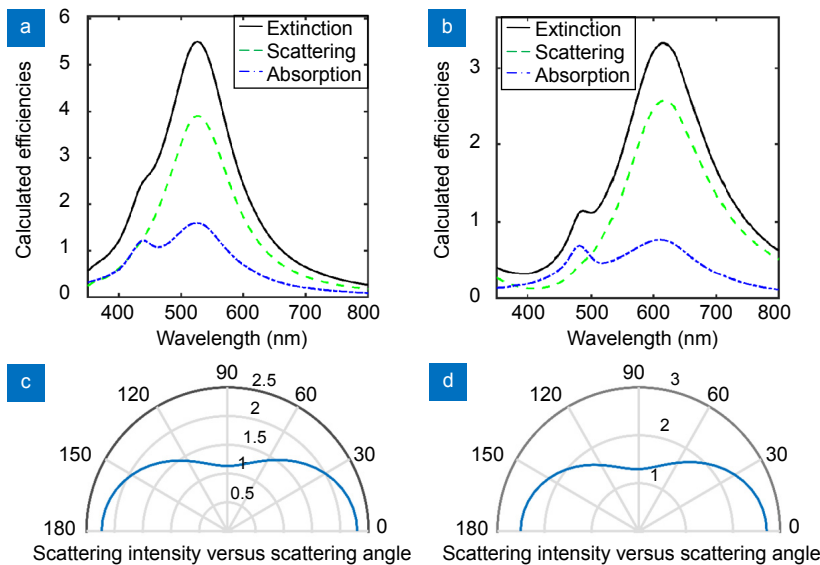


**Fig. 6 | (a)** Optimized results for green light selective scattering. **(b)** Optimized results for red light selective scattering. **(c)** Angular distribution of scattered light for (a) at the wavelength of 525 nm. **(d)** Angular distribution of scattered light for (b) at the wavelength of 620 nm. Efficiency is the corresponding cross section (i.e., extinction, scattering or absorption) divided by the nanoparticle's geometrical cross section  $\pi r^2$ , where  $r$  is core-shell structure's outer radius. The angular distributions of scattered light are calculated by assuming incident light has a unit intensity, and equal components for the p- and s- polarization with respect to the scattering plane. Calculations are done with Mie's theory. Figure reproduced by permission from Ref.<sup>7</sup>, The Royal Society of Chemistry.

diameter of 67 nm and average shell thickness of 18 nm can still be used for selective scattering of green light, as shown later.

Similar to the blue-color-only transparent projection display, a green-color-only transparent projection display film was made by embedding such Ag/TiO<sub>2</sub> spherical nanoparticles into PVA polymer-matrix, and the areal concentration of Ag/TiO<sub>2</sub> nanoparticles is about 9.8 μg/cm<sup>2</sup>. As shown in Fig. 8<sup>7</sup>, the measured extinction, absorption and scattering agree well with the simulated ones.

In Fig. 9<sup>7</sup>, the green-color-only transparent projection display film at work is shown. It can be observed from Fig. 9 that the image of the green letters of “NTU” projected onto the film is very clear (Fig. 9(a)). In comparison, the

film without embedding Ag/TiO<sub>2</sub> is very poor (Fig. 9(b)). Meanwhile, the RGB letters placed behind the transparent projection display film can be clearly observed, showing a reasonably high transparency of the film in the visible wavelength range.

### Ellipsoidal plasmonic nanoparticles

In the work reported in Ref.<sup>6</sup>, the suitability of ellipsoidal plasmonic nanoparticles for full-color transparent display was investigated. For the same reason was given in “Method for choosing metal”, Ag is also chosen as the nanoparticles’ constituent material. Apart from the core-shell structures of Silica/Ag and Ag/TiO<sub>2</sub>, the shape of ellipsoid provides an alternative for tuning the resonance wavelength  $\lambda_0$ .

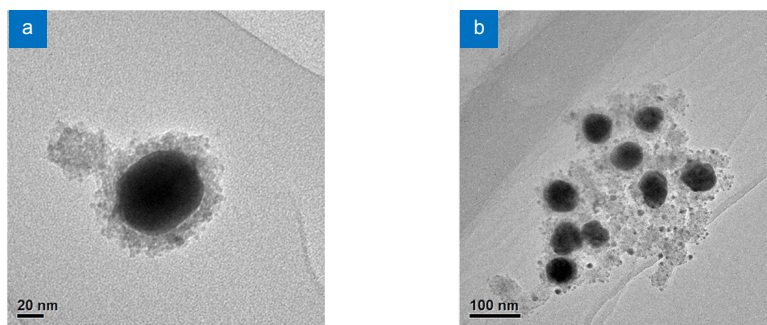


**Fig. 7 | TEM images of the Ag/TiO<sub>2</sub> core-shell structures.** (a) A single core-shell structure, and (b) multiple core-shell structures surrounded by some free TiO<sub>2</sub> nanoparticles. The average values of the core diameters and shell thicknesses are 67 nm and 18 nm, respectively. Figure reproduced by permission from Ref.<sup>7</sup>, The Royal Society of Chemistry.

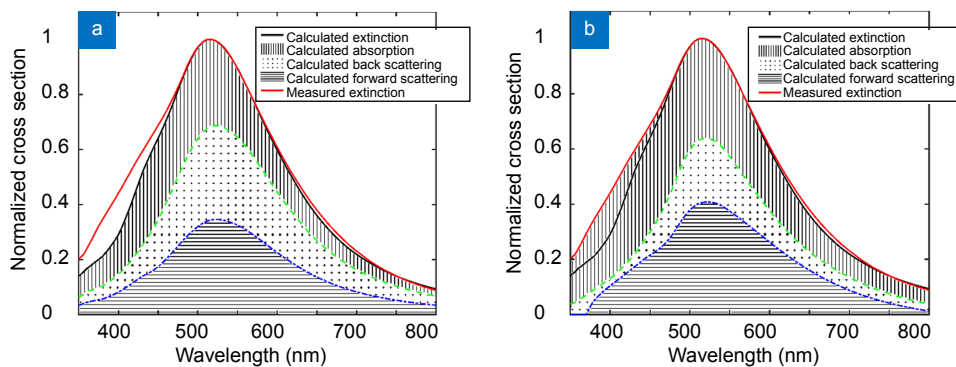


**Fig. 8 | Comparison between (a) the theoretically calculated cross sections of absorption, and forward and backward scattering and (b) experimentally measured ones.** Note that comparison between the calculated extinction (the solid black line) and measured extinction (the solid red line) is shown in both (a) and (b). Figure reproduced by permission from Ref.<sup>7</sup>, The Royal Society of Chemistry.

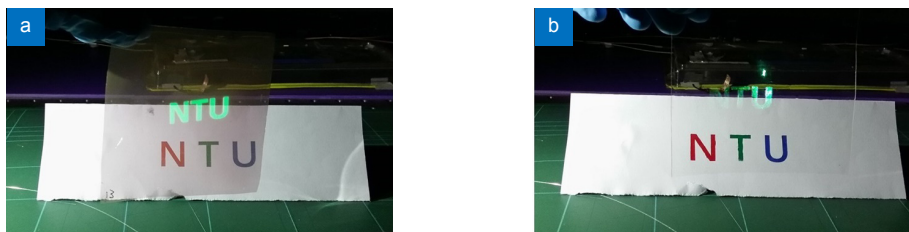


**Fig. 9 | (a) Image projected on the transparent projection display film that is fabricated by dispersing Ag/TiO<sub>2</sub> into PVA. (b) A comparison film made of PVA without dispersion of Ag/TiO<sub>2</sub>.** A laser projector (SONY MP-CL1A) is used for projection. In the projection experiment, green light with a wavelength of 523±3 nm is used. Figure reproduced by permission from Ref.<sup>7</sup>, The Royal Society of Chemistry.

The geometry array under consideration is shown in Fig. 10<sup>6</sup>, which is composed of a bi-dimensional periodic array of Ag ellipsoids arranged in a square lattice and surrounded by a transparent dielectric matrix with dielectric constant of  $\epsilon_h$ . The distance between two adjacent Ag ellipsoids' geometric centres is denoted with  $d$ , and is equal to 100 nm. The major semi-axis along the  $y$ -axis of the ellipsoids is denoted as  $a$ , and the two minor semi-axes  $b, c$  of the ellipsoids are assumed to be equal. The propagation direction of the incident light is assumed to be normal to the plane of the periodic array, and electric field oscillation of incident light is along the major semi-axis (i.e., a TE-plane wave).

Effect of surface scattering is taken into account in the same way as described in section "Ag/TiO<sub>2</sub>", i.e., equations (4) and (5) are applicable to the ellipsoidal plasmonic

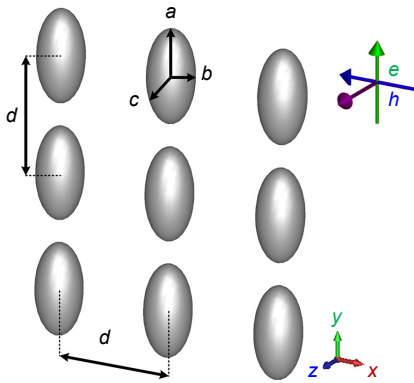


**Fig. 10 | The proposed geometry array of Ag ellipsoids.** Ellipsoids are arranged in a square lattice and illuminated by incident light with its electric field aligned parallel to the major axis of the ellipsoids (i.e., TE-plane wave illumination).  $d$  is the separation distance between the centres of two adjacent nanoparticles, while  $a, b$  and  $c$  are the major and minor axes of the ellipsoids, respectively. Figure reprinted with permission from Ref.<sup>6</sup>, AIP Publishing.

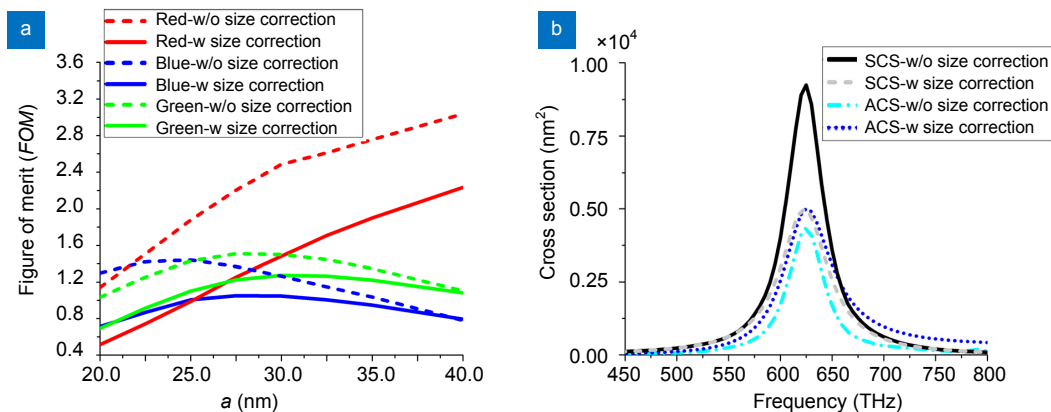


**Fig. 11 | (a)** Initial optimization of Ag ellipsoids for selective scattering of the three basic additive colours (red, green and blue) based on  $FOM$ . For each basic array of Ag ellipsoids, the nanoparticles' major axis is varied from 20 nm to 40 nm while their eccentricity is fixed at 0.96, 0.9, and 0.81 for the red, green, and blue arrays, respectively. As a comparison, values of the  $FOM$  without consideration of effect of surface scattering of conduction electrons are also shown (dashed lines). **(b)** Calculated cross sections for scattering (SCS) and absorption (ACS) for a Ag ellipsoids array with the following parameters:  $a=20$  nm,  $b=c=12$  nm, and  $d=100$  nm. Both results with and without consideration of surface scattering of free electrons (i.e., the size-correction) are shown. Figure reprinted with permission from Ref.<sup>6</sup>, AIP Publishing.

nanoparticles here; however, equation (5) is slightly modified to account for difference between major and minor axes of ellipsoid, as given by the equation below:

$$\gamma_s^i = \frac{A v_F}{r_i} \quad (6)$$

where  $i(=a, b$  or  $c)$  represents the major semi-axis along  $y$ -axis or the two minor semi-axes of the ellipsoids, i.e.,  $r_a=a, r_b=r_c=b$ , and  $A$  is a correction factor. From equation (6), it is obvious that damping of free electrons along the major axis of ellipsoid is different from that along the minor axes. Therefore, the dielectric function of an ellipsoidal Ag nanoparticle is slightly anisotropic.

Through an analytical model<sup>29-33</sup>, it is concluded that resonance peak wavelength of a Ag ellipsoid is mainly affected by eccentricity, and that a trade-off between sharpness of scattering peak (i.e., frequency-selectivity of scattering) and light absorption level cannot be avoided when adjusting its size. And it is found that the eccentricity is equal to 0.96, 0.9, and 0.81 for the red, green, and blue arrays, respectively. Therefore, as a first estimation, it is useful to fix eccentricity of a set of Ag ellipsoids to 0.96, 0.9 or 0.81 and tune their major axis  $a$  to maximize  $FOM$  defined by equation (3). The result of this initial maximization is shown as solid lines in Fig. 11(a)<sup>6</sup>.

For the nanoparticles array resonating in the red region, significantly higher  $FOM$  values can be observed in Fig. 11(a). This is mainly due to the fact that a non-neglectable portion of the scattering and absorption response of these arrays falls at the infrared wavelengths, and, thus, is excluded by the  $FOM$  computation.

In Fig. 11(a)<sup>6</sup>,  $FOM$  calculated without considering surface scattering of conduction electrons (i.e., directly use Ag's dielectric constants from the literature)<sup>19</sup> are also shown as dashed lines. It is clear that at smaller sizes, values of  $FOM$  calculated without surface scattering are much larger than those calculated with surface scattering.

An intuitive understanding is gained from Fig. 11(b)<sup>6</sup>, where scattering and absorption spectrums are calculated for a nanoparticle array designed to resonate in the blue region ( $a=20$  nm,  $b=c=12$  nm, and  $d=100$  nm) with and without surface scattering. From Fig. 11(b)<sup>6</sup>, it is clear that without consideration of surface scattering, scattering level is overestimated, and absorption level is underestimated.

Starting from the initially optimized results shown in Fig. 11(a)<sup>6</sup>, the final optimized Ag ellipsoids for red, green and blue light selective scattering are shown in Table 3.

**Table 3 | Optimal particle sizes and FOM for ellipsoidal Ag nanoparticles.**

Wavelength $\lambda_0$	$a$	$b$	FOM
461 nm	25 nm	17 nm	0.93
530 nm	26 nm	13 nm	1.1
678 nm	30 nm	9 nm	1.6

Table adapted with permission from Ref.<sup>6</sup>, AIP Publishing.

Since the optimized ellipsoidal Ag nanoparticles in Table 3 are obtained by assuming incident light to be TE-plane wave, the design shown in Fig. 12 is proposed

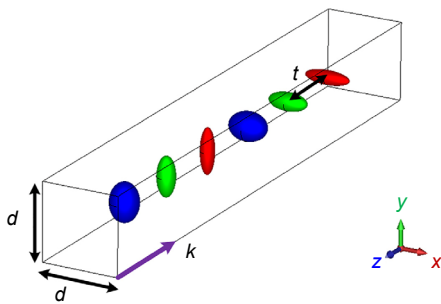


**Fig. 12 | Proposed unit-cell of a full-color and almost polarization-independent transparent projection display screen achieved with Ag ellipsoid arrays.** The propagation direction of the incident light is along the negative direction of the z-axis. This unit-cell repeats itself in the  $x$ - $y$  plane along the  $x$ - and the  $y$ -axes with period  $d=100$  nm. Each unit cell consists of two replicas of each of the optimized nanoparticle array shown in Table 3, and one set is rotated by  $90^\circ$  relative to the other, with adjacent layers separated by a distance  $t$ . Figure reprinted with permission from Ref.<sup>6</sup>, AIP Publishing.

to realize a full-colour and almost polarization-independent transparent projection display<sup>6</sup>.

The full-wave results of the proposed structure depicted by Fig. 12 are shown in Fig. 13<sup>6</sup>, where results for both polarizations of incident light (i.e., oscillating electric field along the  $x$ - and  $y$ -axes) are plotted.

As observed from Fig. 13<sup>6</sup>, the three scattering peaks are sharp, and the overall absorption level is reasonably low. Average transmittance calculated for the TE polarization incidence is 52%. The small differences between results of two incident polarizations are due to residual coupling among different polarizations. The 3D scattering patterns for the TE incident polarization of the optimized Ag ellipsoids in Table 3 are shown in Fig. 14<sup>6</sup>, which indicates that the scattering patterns are almost isotropic.

The simulation in Ref.<sup>6</sup> shows that when half of the ellipsoids in the design in Fig. 12 are randomly shifted up to 15 nm in the  $xy$ -plane, the performance is not affected. Also, for the design in Fig. 12, it is shown that variation of eccentricity up to a minor axis change ratio of 2.5% does not have significant effect on performance. Thus, it is believed that the design in Fig. 12 has some robustness towards geometrical imperfections.

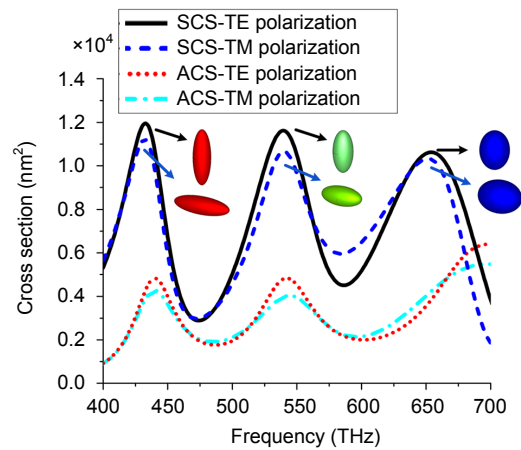


**Fig. 13 | Scattering (SCS) and absorption (ACS) cross sections calculated for the display screen proposed in Fig. 12 under incident light with TE or TM polarization.** Figure reprinted with permission from Ref.<sup>6</sup>, AIP Publishing.

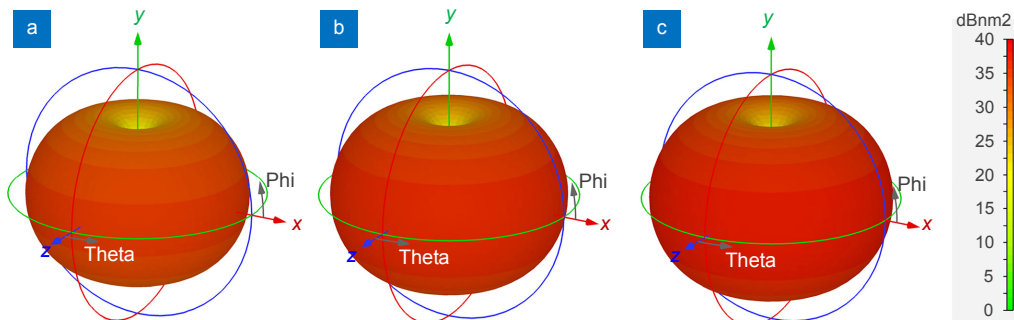


**Fig. 14 | 3D angular scattering distribution for the optimized Ag ellipsoids in Table 3: (a) Ag ellipsoid array for red light scattering, (b) Ag ellipsoid array for green light scattering and (c) Ag ellipsoid array for blue light scattering.** Scale is the same for all subfigures. Figure reprinted with permission from Ref.<sup>6</sup>, AIP Publishing.

Super-sphere core-shell

Apart from spherical core-shell nanoparticles, the structure of super-sphere core-shell nanoparticle is also proposed with silica as core, and Ag as shell<sup>34</sup>, as shown in Fig. 15<sup>34</sup>. Super-sphere, as shown in Fig. 15(a)<sup>34</sup>, is an intermediate shape between sphere and cube, and its surface is described by the following equation in the 3-dimensional cartesian coordinate system<sup>35</sup>:

$$|x|^p + |y|^p + |z|^p = a^p, \quad (7)$$

where  $a$  is the radius of the super-sphere, and  $p$  (called polyhedricity parameter) controls the degree the super-sphere tends towards a perfect cube (a perfect sphere when  $p=2$ , and a perfect cube when  $p=\infty$ ). When  $p>2$ ,  $2a$  is the edge length of the rounded nanocube. As shown in Fig. 15(b)<sup>34</sup>, for a general super-sphere core-shell nanoparticle ( $p>2$ ) with silica as core and Ag as shell, the inner silica-core is a super-sphere with radius of  $a_1$ , and the outermost surface of the Ag shell is a super-sphere with radius of  $a_2$ .

Under quasi-static limit ( $2a_2 \ll \text{wavelength of incident light}$ ), the peak wavelength of resonant scattering and strength of scattering cross section are controlled by tuning  $p$  and the ratio  $a_1/a_2$ . From a simplified polarizability model of the super-sphere core-shell nanoparticle<sup>36</sup>, one can find the optimum ratio  $a_1/a_2$  that maximizes the na-

noparticle's polarizability at the three central wavelengths for blue, green and red light with  $p$  assumed to be 2 (perfect sphere case). After that, values of  $a_1/a_2$  are fixed at the optimum ones from the previous step, while  $p$  is varied from 2 to 20 to optimize scattering cross section and absorption cross section at the three desired central wavelengths for blue, green and red light. The reason why upper limit of  $p$ 's adjusting range is 20 is that 20 is large enough for the super-sphere to be treated as a cube, and further increasing  $p$  does not impose a significant change on the peak wavelength and scattering cross section.

The optimized results of the scattering cross section and absorption cross section are shown in Fig. 16<sup>34</sup>, and the corresponding nanoparticle structures and 3-dimensional scattering angular distributions are shown in the insets of the figure.

The main advantage of super-sphere is that when varying  $p$  to increase scattering cross section, the nanoparticle's absorption cross section remains almost unchanged. Thus, the structure of super-sphere core-shell is a promising solution for suppressing light absorption while achieving strong frequency-selective light scattering. But its disadvantage is also obvious, i.e., the fabrication procedure should be carefully designed to control geometrical deviations from designed ones.

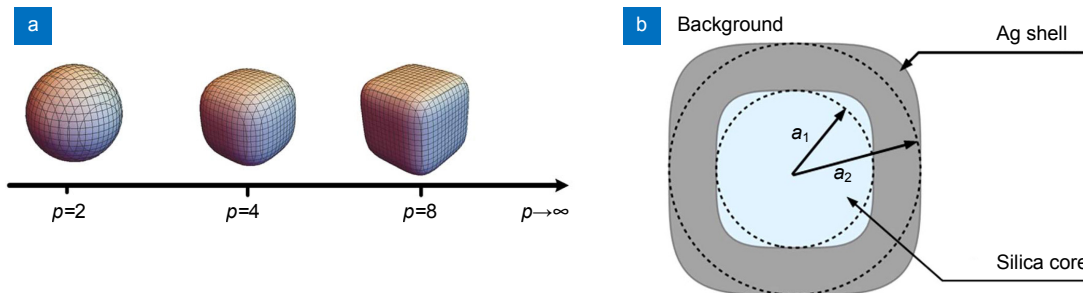


**Fig. 15 |** (a) Schematic sketch of the shapes of super-sphere. The surface of the super-sphere is described by equation (7). Increasing polyhedricity parameter  $p$  will make a super-sphere approach to the shape of a cube. (b) Schematic of a super-sphere core-shell structure, with silica as core and Ag as shell.  $a_1$  and  $a_2$  are the inner and the outer radius of super-spheres, respectively. Dashed lines indicate the special case of the super-sphere core-shell structure when  $p=2$ , i.e., the perfect spherical case. Figure adapted with permission from Ref.<sup>34</sup>, Optical Society of America.

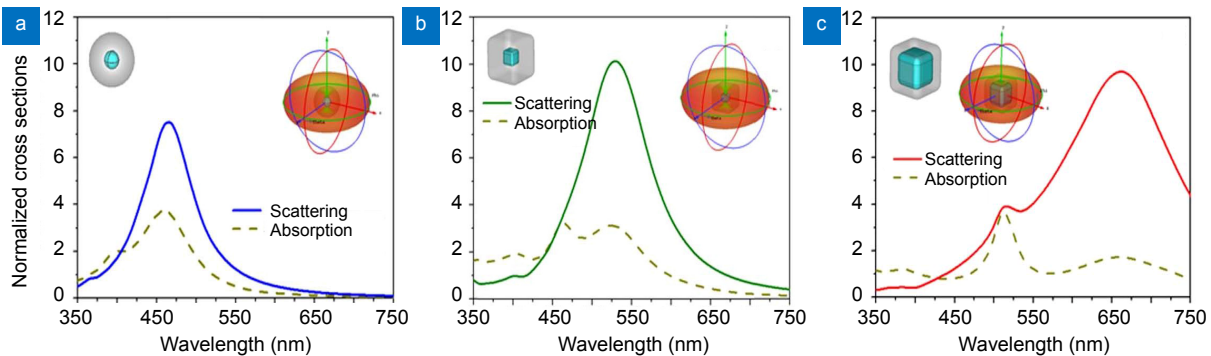


**Fig. 16 |** (a) Optimized results of super-sphere for blue light selective scattering,  $a_1=10$  nm,  $a_2=30$  nm,  $p=2$ . (b) Optimized results of super-sphere for green light selective scattering,  $a_1=10$  nm,  $a_2=30$  nm,  $p=7$ . (c) Optimized results of super-sphere for red light selective scattering,  $a_1=44$  nm,  $a_2=30$  nm,  $p=6$ . Insets show structures' corresponding geometric schematics and angular distribution of scattering. Figure adapted with permission from Ref.<sup>34</sup>, Optical Society of America.

## Metallic nanocubes

The structure of metallic nanocube may provide another alternative for selective scattering<sup>5,37,38</sup>. From “Method for choosing metal”, it is not surprising that Ag is chosen as the constituent material for metallic nanocube again.

As shown in Fig. 17<sup>39</sup>, when a Ag nanocube is placed on a solid dielectric substrate, its LSPR light scattering peak splits into two modes: the distal mode (peak 1) and the proximal mode (peak 2). And it has been shown that the higher the refractive index of the substrate, the larger the distance between the two peaks<sup>39</sup>. As will be shown later, when TiO<sub>2</sub> which has high refractive index is chosen as the substrate, the peak at lower wavelength is suitable for selective backscattering of blue light.

The resonance peak splitting of a Ag nanocube, also called Fano resonance, when it is placed on a dielectric substrate originates from the substrate-mediated coupling between a bright dipolar and a dark quadrupolar plasmon mode<sup>40,41</sup>.

Both peak wavelength and intensity of scattering spectrum are affected by nanoparticle's size<sup>8,9</sup>, which is confirmed by the results shown in Fig. 18(a)<sup>5</sup>. In this figure, the backscattering spectrums of Ag nanocubes with three different sizes (edge lengths of 80 nm, 100 nm and 120 nm

nm) on sufficiently thick TiO<sub>2</sub> (800 nm) were simulated using Lumerical FDTD solutions<sup>5</sup>.

Based on the results shown in Fig. 18(a)<sup>5</sup>, it can be concluded that Ag nanocube with a 100 nm edge length is more suitable for transparent projection display due to the following two reasons: 1. The two peak wavelengths of its scattering peaks are around 440 nm and 640 nm, respectively, which are more suitable for blue and red light scattering. 2. It is more difficult to synthesize nanocube of larger sizes. It is believed that enhancement of green light backscattering is not so important since human eyes are sensitive to green light (see the photopic luminous curve in Fig. 18(a)). As observed from Fig. 18(a)<sup>5</sup>, backscattering of red light is much weaker compared to that of blue light, so it is desirable to enhance backscattering of red light. If more red light is reflected at the air/TiO<sub>2</sub> interface, then more red light is expected to be scattered by Ag nanocube, and hence backscattering of red light is expected to be enhanced. Reflection of red light can be increased by taking advantage of constructive optical interference: make the red light reflected at the air/TiO<sub>2</sub> interface constructively interfere with that reflected at the TiO<sub>2</sub>/glass interface (the substrate is assumed to be glass). The light intensity that the Ag nanocube receives may be

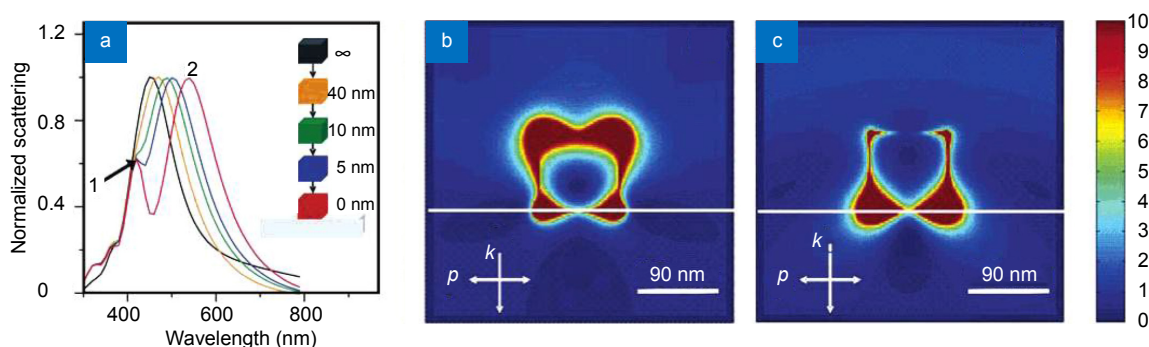


**Fig. 17 |** FDTD (finite-difference time-domain) simulations showing (a) a second peak emerges when a single Ag nanocube (edge length of 90 nm) approaches a glass substrate (index assumed to be 1.5), and the near field  $|E|$  plots for (b) peak 1 and (c) peak 2 of the nanocube placed on the glass substrate. The surrounding medium is air, and the white line in (b), (c) represent the interface between Ag nanocube (or Air) and the glass substrate. Figure adapted with permission from Ref.<sup>39</sup>, American Chemical Society.

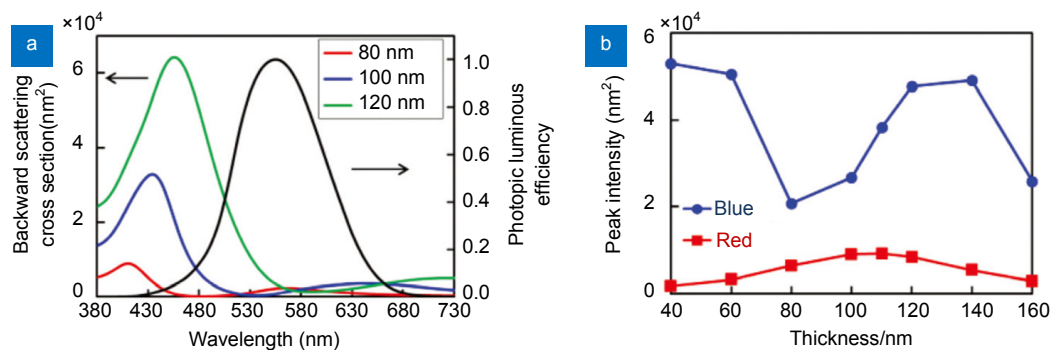


**Fig. 18 |** (a) Simulated backward scattering spectrums with FDTD for Ag nanocubes deposited on TiO<sub>2</sub> with sufficient thickness (800 nm). The luminosity function is also shown to indicate that human eyes are not sensitive to blue and red light. In the calculations, TiO<sub>2</sub>'s refractive index is from Ref.<sup>42</sup>, and Ag's refractive index is from Ref.<sup>19</sup>. (b) Calculated dependence of the distal and proximal mode backward scattering peak intensities of a 100 nm Ag nanocube on the TiO<sub>2</sub> thickness. Figure reproduced with permission from Ref.<sup>5</sup>, The Royal Society of Chemistry.

altered in some cases by the existence of the nanocube itself. Therefore, the backscattering cross sections of the Ag nanocube (100 nm of edge length) on TiO<sub>2</sub> films of different thicknesses have been calculated and are plotted in Fig. 18(b) to find out the appropriate TiO<sub>2</sub> thickness<sup>5</sup>. It can be concluded from the figure that the thickness of 110 nm is the most suitable, since at this film thickness, backscattering of red light is the strongest and backscattering of blue light is reasonably high.

In Ref.<sup>5</sup>, following the theoretical considerations, experimental verification was conducted. TiO<sub>2</sub> thin film with a thickness of 110 nm was deposited on one side of a piece of borosilicate glass slip. Then, Ag nanocubes with an average edge length of 100 nm were synthesized and deposited on the TiO<sub>2</sub> thin film (areal density is around  $3.5 \times 10^8$  particles per cm<sup>2</sup>). The Ag nanocubes were deposited on the TiO<sub>2</sub> thin film by casting an ethanolic dispersion of the nanocubes followed by evaporation of ethanol and a rinse with deionized water. The measured backscattering spectrum and transmittance spectrum of the experimentally prepared sample are shown in Figs. 19(a) and 19(b)<sup>5</sup>, respectively.

Figure 20 shows the display sample at work (a) and its transparency where no image is projected (b)<sup>5</sup>.

From both Figs. 18(a) and 19(a)<sup>5</sup>, it is obvious that backward scattering of blue light is stronger than that of red light. But from Fig. 20<sup>5</sup>, the red colour of the project-

ed image does not seem to be weaker than blue colour. This contradiction originates from the viewing angle (assuming normal projection, the angle between normal of the display sample and the viewing direction), as explained in the following. When the viewing angle increases, backward scattering of red light increases while backward scattering of blue light decreases. Since the picture in Fig. 20 is taken at a large viewing angle, visual perceiving of red light and blue light is rather balanced.

On top of the results shown in Figs. 18(a) and 19(a)<sup>5</sup>, it is of interest to further enhance backscattering of red light. For this purpose, two solutions have been proposed in another work<sup>38</sup>. Through simulations of Ag nanocubes of different sizes placed on TiO<sub>2</sub> substrate, it is found that when Ag nanocubes and the projector are on different sides with respect to the air/TiO<sub>2</sub> interface, backward scattering of red light is stronger than that of blue light, as shown in Fig. 21(b)<sup>38</sup>. Similar simulation studies on Au nanocubes placed on glass substrate indicate that Au nanocube can enable strong enhancement of backward scattering of red light when Au nanocubes and the projector are on different sides with respect to the air/glass interface, as shown in Fig. 21(d)<sup>38</sup>.

Based on the results shown in Fig. 21, two solutions for simultaneous backward scattering of blue and red light were proposed<sup>38</sup>. The insets of Fig. 22<sup>38</sup> show the schematics of the two proposed solutions. The corresponding

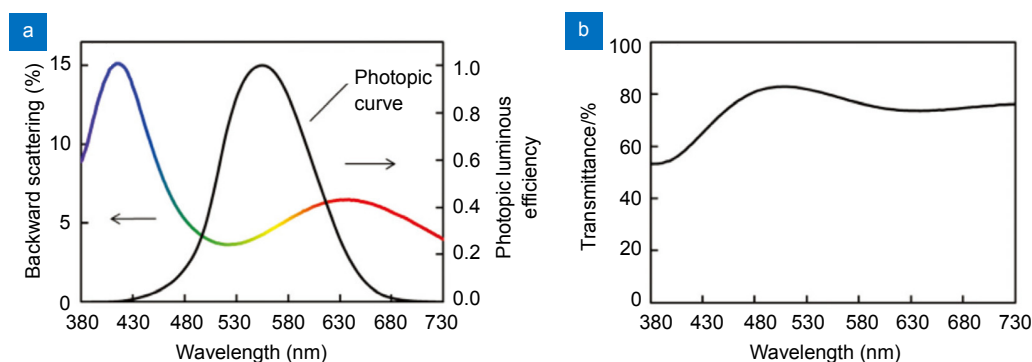


**Fig. 19 | (a) Backward scattering spectrum and (b) transmittance spectrum of the transparent projection display sample experimentally prepared by depositing a monolayer of Ag nanocubes (with average edge length of 100 nm) on the film of TiO<sub>2</sub> with thickness of 110 nm. The TiO<sub>2</sub> film is deposited on glass substrate. The luminosity function is also shown in (a). Figure reproduced from Ref.<sup>5</sup> with permission from The Royal Society of Chemistry.**

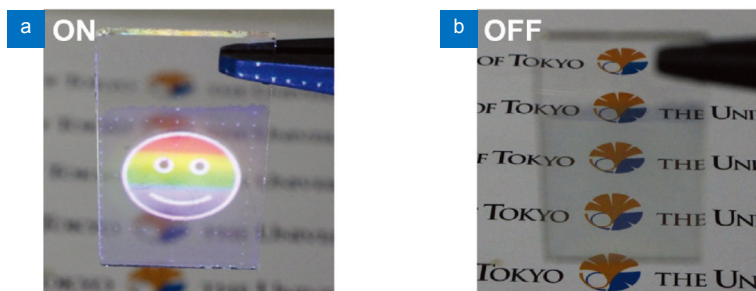


**Fig. 20 | (a) A colourful image is projected onto the display sample using an LCD projector (Epson EB-1761W, peak wavelengths of blue, green, and red light are at 442, 552, and 612 nm, respectively). (b) Transparency of the display sample when no image is projected. Figure reproduced with permission from Ref.<sup>5</sup>, The Royal Society of Chemistry.**

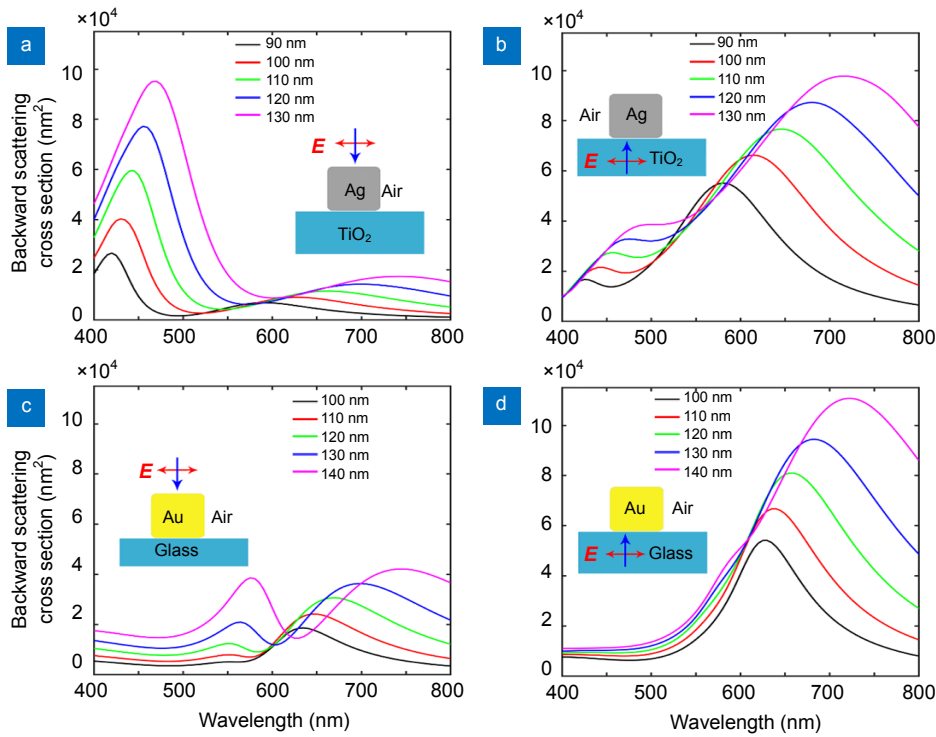


**Fig. 21 | Backward scattering cross sections simulated with FDTD for Ag and Au nanocubes placed on dielectric substrate.** Incident light polarization and propagation direction are shown by each sub-figure's inset. The legends denote edge lengths of nanocubes. (a) Ag nanocubes placed on  $\text{TiO}_2$  substrate with incident light coming from air. (b) Ag nanocubes placed on  $\text{TiO}_2$  substrate with incident light coming from  $\text{TiO}_2$  substrate. (c) Au nanocubes placed on glass substrate with incident light coming from air. (d) Au nanocubes placed on glass substrate with incident light coming from glass substrate. Figure reproduced with permission from Ref.<sup>38</sup>, The Electrochemical Society.

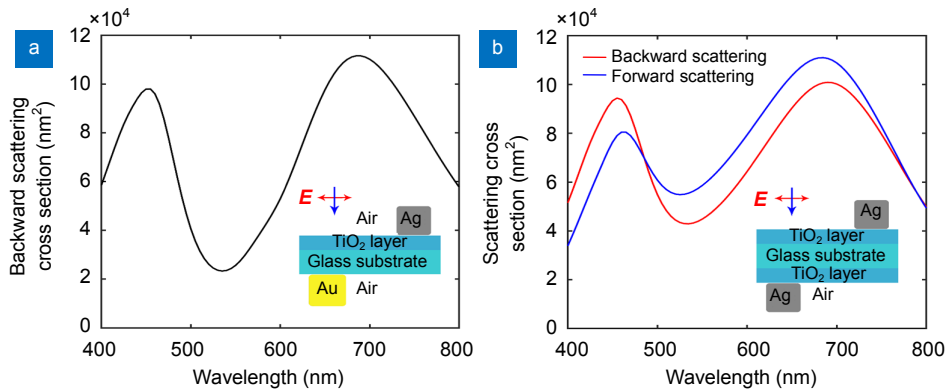


**Fig. 22 | Simulated results of the two proposed solutions to enhance backward scattering of red light.** The setups are schematically illustrated by insets. (a) Ag nanocube's edge length is 120 nm, Au nanocube's edge length is 130 nm, and  $\text{TiO}_2$  film's thickness is 137 nm. (b) The edge length of Ag nanocubes on both sides is 120 nm, and thickness of the  $\text{TiO}_2$  films on both sides is 120 nm. Effect of  $\text{TiO}_2$ 's thickness, and light reflection at all interfaces have been considered. Figure reproduced with permission from Ref.<sup>38</sup>, The Electrochemical Society.

overall backscattering cross sections are also shown in Fig. 22. It is worth mentioning that the solution given in Fig. 22(b) is also capable of forward selective scattering of blue and red light.

### Combination of gain materials with metallic nanoparticles

The widths of selective scattering peaks from the solutions discussed above are much broader than the ideal case shown in Fig. 1<sup>10</sup>, thus it is desirable to further reduce the peak widths (i.e., to increase frequen-

cy-selectivity of scattering). For this purpose, it has been recommended to combine metallic nanoparticles with gain materials<sup>10</sup>. Gain materials have been demonstrated to compensate optical loss, narrow width of resonant scattering peak and even enable lasing state from metallic nanoparticle<sup>43–52</sup>. To combine gain materials with metallic nanoparticles, two core-shell structures have been proposed which are shown in Fig. 23<sup>10</sup>.

The complex refractive index of the silica doped with gain material  $N_{\text{sil}}$  is given by equation (8) (dielectric function is the square of refractive index):

$$N_{\text{sil}} = 1.45 + ik \quad (8)$$

where  $i$  is the imaginary number, and extinction coefficient  $k$  is a negative number for a gain media. Note that for a transparent material,  $k=0$ ; for an absorbing material,  $k>0$ . And the relation between extinction coefficient  $k$  and optical gain is  $gain = -4\pi k/\lambda$ , where  $\lambda$  is the wavelength of the incident light.

With the introduction of gain, the optimization process has one more degree of freedom, i.e., apart from core diameter, shell thickness and resonant wavelength, value of  $k$  can also be tuned. The optimized results are shown in Fig. 24<sup>10</sup>.

From Fig. 24<sup>10</sup>, it is observed that even though the effect of surface scattering of free electrons is considered during optimization (this effect undesirably broadens resonance peak and increases absorption level), including gain materials can achieve very sharp resonant scattering peaks. A comparison between performances of the three structures in Fig. 24 with those of their corresponding ones without gain materials is given in supplementary material to show the significant improvement of scatter-

ing performance with introduction of gain material. Thus, combining gain material with metallic nanoparticles provides a promising way to achieve high frequency-selective light scattering.

## Summary

In this article, for the purpose of achieving transparent projection display, we have reviewed recent progress of frequency-selective scattering of red, green and blue light achieved by metallic nanoparticle's LSPR. Method and criteria of choosing appropriate metal(s) are discussed, and it is concluded that Ag is the most suitable metal in visible wavelength range for the display application. *FOM* is defined to quantify the performance of a designed nanoparticle structure. Selective scattering based on spherical core-shell structures are reviewed. The spherical core-shell structures have the advantage of high symmetry, which means that they do not have the problem of alignment and special requirement on incident light. The structure of ellipsoidal Ag has better performance in terms of *FOM* compared to spherical core-shell structures;

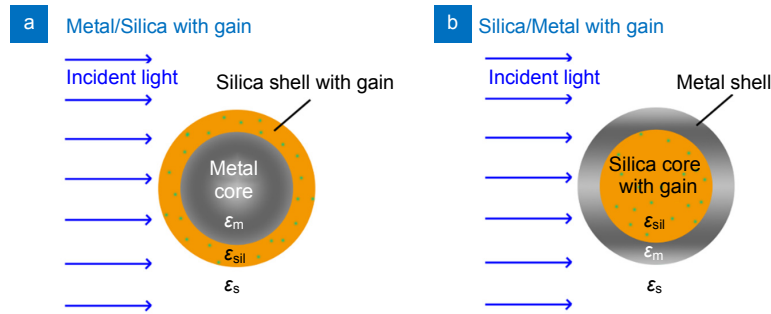


**Fig. 23 | Proposed core-shell structures for combining metallic nanoparticle with gain material.** (a) Core is metal, shell is silica doped with gain material. (b) Core is silica doped with gain material, shell is metal. The surrounding medium's dielectric function  $\epsilon_s$  is assumed to be a constant of 2.25. The complex refractive index of silica doped with gain material is described by equation (8). Metal could be Ag or Au. Figure adapted with permission from Ref.<sup>10</sup>, Optical Society of America.

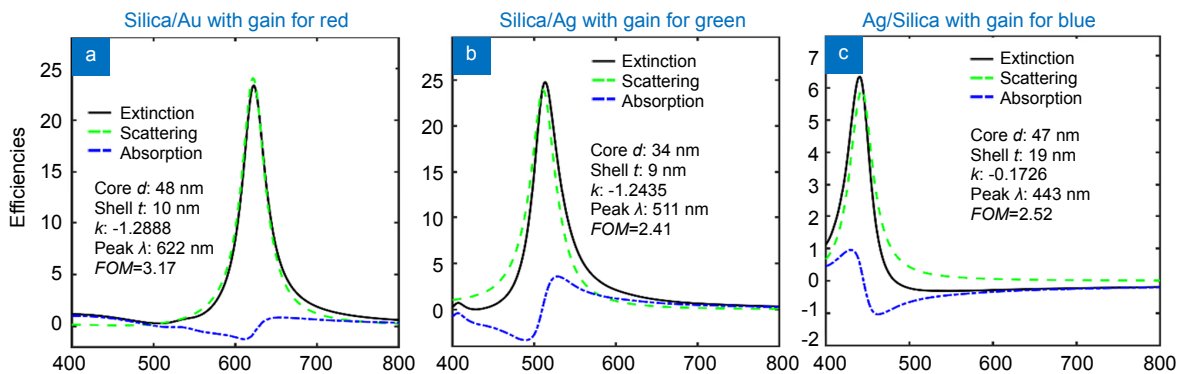


**Fig. 24 | Optimized results for selective scattering of red, green and blue light when gain materials are combined with metallic nanoparticles.** (a) Silica doped with gain material as core, Au as shell, for selective scattering of red light. (b) Silica doped with gain material as core, Ag as shell, for selective scattering of green light. (c) Ag as core, Silica doped with gain material as shell, for selective scattering of blue light. Schematic illustration of core-shell structures is shown in Fig. 23. Optimized parameters and values of *FOM* are shown in the insets. Efficiency is the corresponding cross section (i.e., extinction, scattering or absorption) divided by the nanoparticle's geometrical cross section  $\pi r^2$ , where  $r$  is core-shell structure's outer radius. Simulations are done by the Mie theory<sup>12</sup>. Figure adapted with permission from Ref.<sup>10</sup>, Optical Society of America.

however, due to its asymmetry, extra effort is needed for alignment of nanoparticles to ensure the device's independence on incident light's polarization. Super-sphere core-shell structure provides a promising way of increasing strength of light scattering while suppressing light absorption, but its fabrication process needs careful design to precisely control its geometrical shape. The structure of Ag or Au nanocubes placed on a dielectric substrate provides another alternative for achieving selective scattering, although *FOM* is not suitable to describe its performance. As the selective scattering of the above mentioned structures are not sharp enough, the combination of metallic nanoparticles with gain materials is recommended, which can theoretically generate very sharp scattering peaks.

Much research is still needed to realize commercially viable nanoparticles which have highly frequency-selective scattering of red, green and blue light. And we would like to recommend several future works in this field:

For the three structures proposed in Fig. 24, experimental realization of them is worth trying.

For the idea of placing metallic nanoparticle on dielectric substrate, frequency-selective light scattering properties have only been studied for the shape of nanocube as reviewed in Section "Metallic nanocubes". Therefore, it is recommended that studies on other shapes, such as nano-star, nano-triangle and nano-rice may be attempted. Also, it is interesting to investigate how it will affect their light scattering and absorption properties by coating these nanoparticles with a thin layer of dielectric doped with gain materials. On top of these, it has been shown that when a monolayer of Molybdenum disulfide ( $\text{MoS}_2$ ) is inserted between the metallic nanoparticle and the dielectric substrate, strength and spectral position of the resonance peaks can be tuned by applying different gate voltages on the  $\text{MoS}_2$  monolayer<sup>53</sup>. Therefore, the effect of  $\text{MoS}_2$  monolayer on frequency-selective light scattering properties of metallic nanoparticle deposited on dielectric substrate is worth future research.

Dielectric nanoparticles may be a promising way of achieving frequency-selective scattering of light, as they do not suffer from light absorption as compared to metallic nanoparticle. One example is shown in supplementary material of Ref. 4.

## References

- Jang C, Lee C K, Jeong J, Li G, Lee S *et al.* Recent progress in see-through three-dimensional displays using holographic optical elements. *Appl Opt* **55**, A71–A85 (2016).
- Sun T, Pettitt G, Ho N T, Eckles K, Clifton B *et al.* Full color high contrast front projection on black emissive display. *Proc SPIE* **8254**, (2012).
- Chen S F, Deng L L, Xie J, Peng L, Xie L H *et al.* Recent developments in top-emitting organic light-emitting diodes. *Adv Mater* **22**, 5227–5239 (2010).
- Hsu C W, Zhen B, Qiu W J, Shapira O, DeLacy B G *et al.* Transparent displays enabled by resonant nanoparticle scattering. *Nat Commun* **5**, 3152 (2014).
- Saito K, Tatsuma T. A transparent projection screen based on plasmonic Ag nanocubes. *Nanoscale* **7**, 20365–20368 (2015).
- Monti A, Toscano A, Bilotti F. Analysis of the scattering and absorption properties of ellipsoidal nanoparticle arrays for the design of full-color transparent screens. *J Appl Phys* **121**, 243106 (2017).
- Ye Y Y, Chen T P, Zhen J Y, Xu C, Zhang J *et al.* Resonant scattering of green light enabled by  $\text{Ag@TiO}_2$  and its application in a green light projection screen. *Nanoscale* **10**, 2438–2446 (2018).
- Kreibig U, Vollmer M. *Optical Properties of Metal Clusters* (Springer, Berlin, Heidelberg, 2013).
- Kelly K L, Coronado E, Zhao L L, Schatz G C. The optical properties of metal nanoparticles: the influence of size, shape, and dielectric environment. *J Phys Chem B* **107**, 668–677 (2003).
- Ye Y Y, Liu R Y, Song Z G, Liu Z, Chen T P. Sharp selective scattering of red, green, and blue light achieved via gain material's loss compensation. *Opt Express* **27**, 9189–9204 (2019).
- Kreibig U. Small silver particles in photosensitive glass: their nucleation and growth. *Appl Phys* **10**, 255–264 (1976).
- Quinten M. *Optical Properties of Nanoparticle Systems: Mie and Beyond* (John Wiley & Sons, Weinheim, 2011).
- Yang W. Improved recursive algorithm for light scattering by a multilayered sphere. *Appl Opt* **42**, 1710–1720 (2003).
- Sullivan D M. *Electromagnetic Simulation Using the FDTD Method* 2nd ed (John Wiley & Sons, New Jersey, 2013).
- Draine B T, Flatau P J. Discrete-dipole approximation for scattering calculations. *J Opt Soc Am A* **11**, 1491–1499 (1994).
- Bohren C F, Clothiaux E E. *Fundamentals of Atmospheric Radiation: An Introduction with 400 Problems* (John Wiley & Sons, Weinheim, 2006).
- Kucherenko S, Sytsko Y. Application of deterministic low-discrepancy sequences in global optimization. *Comput Optim Appl* **30**, 297–318 (2005).
- Johnson S G. The NLOpt nonlinear-optimization package. Available from: <https://nlopt.readthedocs.io/en/latest/>, [cited 23rd March 2019, 2019].
- Palik E D. *Handbook of Optical Constants of Solids*, 3. (Academic Press, San Diego, 1998).
- Ye Y Y, Chen T P, Liu Z, Yuan X. Effect of surface scattering of electrons on ratios of optical absorption and scattering to extinction of gold nanoshell. *Nano Res Lett* **13**, 299 (2018).
- Kreibig U, Frangstein C V. The limitation of electron mean free path in small silver particles. *Z Phys* **224**, 307–323 (1969).
- Tang S C, Tang Y F, Zhu S P, Lu H M, Meng X K. Synthesis and characterization of silica–silver core–shell composite particles with uniform thin silver layers. *J Solid State Chem* **180**, 2871–2876 (2007).
- DeVore J R. Refractive indices of rutile and sphalerite. *J Opt Soc Am* **41**, 416–419 (1951).
- Seh Z W, Liu S H, Low M, Zhang S Y, Liu Z L *et al.* Janus Au-TiO<sub>2</sub> photocatalysts with strong localization of plasmonic near-fields for efficient visible-light hydrogen generation. *Adv Mater* **24**, 2310–2314 (2012).
- Mergel D, Buschendorf D, Eggert S, Grammes R, Samset B. Density and refractive index of TiO<sub>2</sub> films prepared by reactive evaporation. *Thin Solid Films* **371**, 218–224 (2000).
- Blaber M G, Arnold M D, Ford M J. Search for the ideal plasmonic nanoshell: the effects of surface scattering and alter-

- natives to gold and silver. *J Phys Chem C* **113**, 3041–3045 (2009).
27. Berciaud S, Cognet L, Tamarat P, Lounis B. Observation of intrinsic size effects in the optical response of individual gold nanoparticles. *Nano Lett* **5**, 515–518 (2005).
28. Scaffardi L B, Tocho J O. Size dependence of refractive index of gold nanoparticles. *Nanotechnology* **17**, 1309–1315 (2006).
29. Park J, Lu W. Orientation of core-shell nanoparticles in an electric field. *Appl Phys Lett* **91**, 053113 (2007).
30. Saeidi C, van der Weide D. Nanoparticle array based optical frequency selective surfaces: theory and design. *Opt Express* **21**, 16170–16180 (2013).
31. Monti A, Alù A, Toscano A, Bilotti F. Optical invisibility through metasurfaces made of plasmonic nanoparticles. *J Appl Phys* **117**, 123103 (2015).
32. Fruhnert M, Monti A, Fernandez-Corbaton I, Alù A, Toscano A *et al.* Tunable scattering cancellation cloak with plasmonic ellipsoids in the visible. *Phys Rev B* **93**, 245127 (2016).
33. Monti A, Toscano A, Bilotti F. Exploiting the surface dispersion of nanoparticles to design optical-resistive sheets and Salisbury absorbers. *Opt Lett* **41**, 3383–3386 (2016).
34. Ramaccia D, Toscano A, Bilotti F. Scattering and absorption from super-spherical nanoparticles: analysis and design for transparent displays [Invited]. *J Opt Soc Am B* **34**, D62–D67 (2017).
35. LAMÉ SURFACE. Available from: <https://www.mathcurve.com/surfaces.gb/lame/lame.shtml>, [cited 25 April 2019].
36. Miyazawa T, Aratake M, Onaka S. Superspherical-shape approximation to describe the morphology of small crystalline particles having near-polyhedral shapes with round edges. *J Math Chem* **50**, 249–260 (2012).
37. Saito K, Tatsuma T. Asymmetric three-way plasmonic color routers. *Adv Opt Mater* **3**, 883–887 (2015).
38. Ye Y Y, Chen T P. Selective scattering of blue and red light based on silver and gold nanocubes. *ECS J Solid State Sci Technol* **8**, R51–R57 (2019).
39. Sherry L J, Chang S H, Schatz G C, Van Duyne R P, Wiley B J *et al.* Localized surface plasmon resonance spectroscopy of single silver nanocubes. *Nano Lett* **5**, 2034–2038 (2005).
40. Davis T J, Gómez D E, Vernon K C. Simple model for the hybridization of surface plasmon resonances in metallic nanoparticles. *Nano Lett* **10**, 2618–2625 (2010).
41. Fang Z Y, Zhu X. Plasmonics in nanostructures. *Adv Mater* **25**, 3840–3856 (2013).
42. Jellison G E Jr, Boatner L A, Budai J D, Jeong B S, Norton D P. Spectroscopic ellipsometry of thin film and bulk anatase (TiO<sub>2</sub>). *J Appl Phys* **93**, 9537–9541 (2003).
43. Avrutsky I. Surface plasmons at nanoscale relief gratings between a metal and a dielectric medium with optical gain. *Phys Rev B* **70**, 155416 (2004).
44. Noginov M A, Zhu G, Bahoura M, Adegoke J, Small C E *et al.* Enhancement of surface plasmons in an Ag aggregate by optical gain in a dielectric medium. *Opt Lett* **31**, 3022–3024 (2006).
45. Digonnet M J F. *Rare-Earth-Doped Fiber Lasers and Amplifiers* 2nd ed (CRC Press, New York, 2001).
46. Lawandy N M. Localized surface plasmon singularities in amplifying media. *Appl Phys Lett* **85**, 5040 (2004).
47. Hide F, Schwartz B J, Diaz-Garcia M A, Heeger A J. Conjugated polymers as solid-state laser materials. *Synth Met* **91**, 35–40 (1997).
48. Gordon J A, Ziolkowski R W. The design and simulated performance of a coated nano-particle laser. *Opt Express* **15**, 2622–2653 (2007).
49. Li X F, Yu S F. Design of low-threshold compact Au-nanoparticle lasers. *Opt Lett* **35**, 2535–2537 (2010).
50. Campbell S D, Ziolkowski R W. Impact of strong localization of the incident power density on the nano-amplifier characteristics of active coated nano-particles. *Opt Commun* **285**, 3341–3352 (2012).
51. Zhang H P, Zhou J, Zou W B, He M. Surface plasmon amplification characteristics of an active three-layer nanoshell-based spaser. *J Appl Phys* **112**, 074309 (2012).
52. Wu D J, Cheng Y, Wu X W, Liu X J. An active metallic nanomatryushka with two similar super-resonances. *J Appl Phys* **116**, 013502 (2014).
53. Li B W, Zu S, Zhou J D, Jiang Q, Du B W *et al.* Single-nanoparticle plasmonic electro-optic modulator based on MoS<sub>2</sub> monolayers. *ACS Nano* **11**, 9720–9727 (2017).

## Acknowledgements

This work is financially supported by National Research Foundation of Singapore (NRF-CRP13-2014-02) and Science and Technology Program of Guangdong Province of China (Project No. 2016A050502058).

## Author contributions

All authors commented on the manuscript. Ye wrote the manuscript. Liu partially contributed to writing of manuscript and helped to revise the manuscript. Chen guided this study and helped to revise the manuscript.

## Competing interests

The authors declare no competing financial interests.

## Supplementary information

Supplementary information for this paper is available at

<https://doi.org/10.29026/oea.2019.190020>